Astron. Astrophys. 351, 292–302 (1999)

ASTRONOMY AND ASTROPHYSICS

Ices and extinction through the Taurus and Ophiuchus clouds

T.C. Teixeira[1,2] **and J.P. Emerson**[1]

[1] Department of Physics, Queen Mary and Westfield College, Mile End Road, London E1 4NS, England, UK (j.p.emerson@qmw.ac.uk)
[2] Institute of Physics and Astronomy, Århus University, Ny Munkegade, 8000 Århus C, Denmark (tct@obs.aau.dk)

Received 28 January 1999 / Accepted 19 August 1999

Abstract. A detailed intercomparison is made between published observations of H_2O and CO ices towards the Taurus and Ophiuchus dark clouds. The column densities of the ices are intercompared, and each compared to the visual extinction through the clouds, A_v. It is neither clear that the two clouds have different or well defined threshold extinctions for the survival of ice mantles, nor that, for each of the clouds, the thresholds for the survival of CO and H_2O mantles are different. The inclusion of new objects in Taurus (Teixeira et al. 1998) introduces a large scatter in the relations between those quantities relative to results obtained by previous authors. Lines-of-sight towards deeply embedded Young Stellar Objects in Taurus appear to show an enhancement in the amount of water-ice relative to lines-of-sight towards field stars behind that cloud. While for $A_v < 14$ mag there is a tight correlation between the water-ice column density, $N_s(H_2O)$, and A_v, the inclusion of those new objects reveals a discontinuity in the relation between $N_s(H_2O)$ and A_v. The interpretation of this discontinuity is discussed.

Key words: stars: formation – ISM: clouds – ISM: dust, extinction – ISM: molecules – infrared: ISM: lines and bands

1. Introduction

Nearby molecular clouds host some of the most well known and intensively studied sites of star formation. Taurus and Ophiuchus are two nearby dark cloud complexes that have attracted interest for many years. Even though the two complexes show similar geometries on both large and small scales (Loren et al. 1990), comparative observational studies point to a number of differences between the properties of star formation occurring in both complexes. It is therefore of interest to use the ices in grain mantles as probes of the conditions in those star forming molecular cloud complexes.

The composition and evolution of interstellar dust has been the subject of intensive observational, laboratory and theoretical efforts, but the composition, structure and size of the dust grains are far from settled (e.g. Tielens & Allamandola 1987a,b, Mathis 1990, 1993, 1998). However, it is clear that dust grains have a refractory (i.e. non-volatile) core containing mostly silicates and carbonaceous material (Tielens & Allamandola 1987b, Williams 1993, Draine 1995), and in molecular clouds acquire mantles of ices on top of their refractory cores.

Infrared spectroscopy has led to the identification of water-ice as the most abundant component of the mantles (Whittet et al. 1988, Eiroa & Hodapp 1989, Tanaka et al. 1990, Tanaka et al. 1994). Solid CO has also been observed to be an important constituent of the ices (Tielens et al. 1991, Kerr et al. 1993, Tanaka et al. 1994, Chiar et al. 1994, 1995, 1998, Teixeira et al. 1998), with an abundance of 10–40% relative to the water-ice. Solid CO_2 is also found in significant amounts in the mantles (d'Hendecourt & de Muizon 1989, de Graauw et al. 1996, Gürtler et al. 1996, Strazzulla et al. 1998, Whittet et al. 1998), and other molecules (such as OCS, CH_4 and SO_2) as more minor constituents of the ices (Palumbo et al. 1997, Boogert et al. 1997). Here we will only be concerned with H_2O and CO ices, since these are the only ices for which systematic studies of both Taurus and Ophiuchus are currently available.

Previous studies suggested linear relations between the column densities of CO and H_2O, and between the column density of each of those ices and the visual extinction, A_v, for lines-of-sight towards Taurus (e.g. Whittet et al. 1988, Tanaka et al. 1994, Chiar et al. 1995, and references therein). The existence of linear relations between the ices' column densities and the visual extinction to the objects has been the main argument in deciding between two scenarios for the distribution of the ices in molecular clouds (Schutte 1996): *(i)* different types of ices (namely H_2O- and CO-ices) are segregated and reside in spatially separate regions in the cloud, or *(ii)* the different ices are well mixed within the cloud and possibly coexist in the ice mantle of each coated grain in an "onion-shell" structure. The observed linear relations point to scenario *(ii)*, with the column density of each of the ices being directly proportional to the column density of ice-coated grains in the line-of-sight (Whittet et al. 1988, Sato et al. 1990).

This work shows that the assumption of the existence of such linear relations is not warranted by the currently available data. The paper starts by assuming the linear relations exist, to conclude, after a thorough analysis of the scatter in the plots, that the scatter cannot easily be explained by observational uncertainties and that therefore the linear relations might not apply

Send offprint requests to: T.C. Teixeira

throughout. Sect. 2 deals with the relation between the column densities of CO and H_2O. The relation between the column densities of the ices and the visual extinction, A_v, is analysed in Sect. 3. The interpretation of the results is presented in Sect. 4, where the implications of the existence or not of linear relations are discussed, as well as an alternative interpretation of the plots. The conclusions are summarized in Sect. 5.

2. Examining the abundances of the ices: CO and H_2O

To date, all observations of ices in molecular clouds have shown that water-ice is observed in all lines-of-sight where CO-ice has been observed. The reverse is not true and previous studies (e.g. Tanaka et al. 1994, Chiar et al. 1995) examined the abundances of these ices in molecular clouds in an attempt to find a (cor)relation between them. In view of new data for embedded Young Stellar Objects (hereafter YSOs) (Teixeira et al. 1998), that analysis will be updated here for Taurus and Ophiuchus.

2.1. The sample of objects: column densities of the ices

The solid CO and H_2O column densities (N_s(CO) and $N_s(H_2O)$, respectively) of all embedded YSOs and field stars towards Taurus and Ophiuchus where one or both of those ices have been searched for are presented in Table 1. The sources' approximate coordinates are also given in that table.

Solid CO column densities were (re)calculated from published observations, where available (cf. Teixeira 1998). For the calculation of the water-ice column densities observations of the 3.05 μm band were used. The peak optical depths and full width at half maximum (FWHM) of the features were taken from the literature, where available, and the column densities were calculated using the following expression (e.g. d'Hendecourt & Allamandola 1986):

$$N \cong \frac{\tau_{\max}.\Delta\nu_{1/2}}{A} \text{ which follows from } N = \frac{\int \tau_\nu \, d\nu}{A} \qquad (1)$$

for a near Lorentzian shaped band. $\tau_{\max}$ represents the peak optical depth of the feature, $\Delta\nu_{1/2}$ is the FWHM (cm^{-1}) of the feature with the spectrum in optical depth units, and A is the integrated band absorbance (cm/molecule). In the case of the OH stretch of the H_2O molecule at 3.05 μm (3275 cm^{-1}), $A = 2.0 \times 10^{-16}$ cm/molecule (d'Hendecourt & Allamandola 1986).

Where $\tau_{\max}$ and/or $\Delta\nu_{1/2}$ were not stated in the literature, they were estimated from the published spectra. In some cases a FWHM had to be assumed. As the peak optical depth and the FWHM of the 3.05 μm feature might be correlated (Teixeira 1998), we did not to use the average of the observed values of $\Delta\nu_{1/2}$. Instead, $< \Delta\nu_{1/2} > \simeq 360\,cm^{-1}$ appears to provide a lower limit for the features observed towards embedded objects, and an upper limit for the features observed towards field stars. In this way, any possible differences between the features observed towards field stars and embedded objects are not artificially enhanced.

The solid-CO upper limits in Table 1 were estimated using $A = 1.1 \times 10^{-17}$ cm/molecule. The FWHM was assumed to be $< \Delta\nu_{1/2} > \sim 8\,cm^{-1}$, which corresponds to the width of the broadest features towards Taurus.

The uncertainties in the water-ice column density were estimated by taking the uncertainty in the optical depth and an assumed uncertainty of 30 cm^{-1} in the FWHM. The uncertainties in the column densities of both solid H_2O and solid CO are likely to be underestimated for a number of reasons. The choice of the continuum affects both the peak optical depth and the FWHM of the feature. As shown by Gerakines et al. (1995), in both cases (H_2O and CO) the value of the integrated band absorbance, A, is dependent on the exact composition of the ice and on its temperature. The dependence is weak, never exceeding 20% of the value of the band strength for the pure ice. The uncertainty in all column densities is, at best, $\sim$ 15%. In all calculations that follow the uncertainty in each column density will be taken from Table 1 if in excess of 15%, and will otherwise be set to 15%.

Further details of particular assumptions made on individual sources may be found in Teixeira (1998).

2.2. CO-ice versus H_2O-ice

A plot comparing the abundances of the ices towards different lines-of-sight is one of the tools that can help visualize differences between different clouds and different kinds of objects (Tanaka et al. 1994, Chiar et al. 1995). Fig. 1 is a plot of the solid-CO column density against the solid-H_2O column density for all the lines-of-sight in Table 1. Comparison with Fig. 2 in Chiar et al. (1995) shows that the new points in Taurus introduce a large scatter in the diagram. Three observations can be made: *(i)* the embedded objects in Taurus do not follow the same trend as the field stars, *(ii)* there is a large scatter for the embedded sources in Ophiuchus (see also Chiar et al. 1995), but they do not appear to follow the trend of the embedded sources in Taurus, *(iii)* above a solid-H_2O column density ($\sim 1.5 \times 10^{18}\,cm^{-2}$) the amount of solid-CO in the line-of-sight seems to suddenly increase with an accompanying increase of the scatter. Whilst points *(i)* and *(ii)* are drawn from the joint plot (Fig. 1), point *(iii)* is more apparent if the plots for Taurus and Ophiuchus are presented separately (Fig. 2a and b).

A linear least squares fit taking into account the uncertainties in both coordinates (Press et al. 1992) results in the following relation for the field stars in Taurus (excluding the upper limits):

$$\begin{aligned} N_s(CO) \;=\; & (0.37 \pm 0.07) N_s(H_2O) \\ & + (-1.3 \pm 0.8) \times 10^{17}\,cm^{-2} \end{aligned} \qquad (2)$$

and corresponds to the dashed line in Fig. 1. The positive intercept on the x-axis is estimated[1] to be $N_s(H_2O) = (3.6 \pm 1.4) \times 10^{17}\,cm^{-2}$, which is the amount of water-ice present in an outer

[1] The x-axis intercepts mentioned in this section were obtained by constructing linear least-squares fits to the data taking the column densities of CO as abscissae and the column densities of H_2O as ordinates. This is because it is more robust to obtain the value of the intercepts (with uncertainties) directly from the data points, rather than indirectly from (2).

Table 1. Coordinates, solid-CO and solid-H_2O column densities (N_s(CO) and $N_s(H_2O)$, respectively), and visual extinction, A_v, towards embedded YSOs and field stars in and behind the Taurus and Ophiuchus molecular clouds. The meaning and uncertainties of the remaining symbols is discussed in Sect. 2.

Object	$\alpha(2000)^a$	$\delta(2000)^a$	$N_s(CO)$ (10^{17} cm^{-2})	Ref.^{g}	τ_{H_2O}	FWHM (cm^{-1})	$N_s(H_2O)$ (10^{18} cm^{-2})	Ref.^{g}	A_V
Taurus, YSOs									
Elias 1	04 18 40.7	+28 19 16	0.85 ± 0.03	1	0.51 ± 0.08	360^d	0.92 ± 0.14	7	10.5
Elias 7	04 29 23.8	+24 33 02	1.2 ± 0.6	4	0.42 ± 0.05	360^d	0.76 ± 0.11	8	11.4
Elias 18	04 39 55.7	+25 45 02	3.10 ± 0.02	1	0.88 ± 0.03	360^d	1.6 ± 0.1	8	19.4
Elias 23	04 32 15.4	+24 29 00	< 0.7	4	0.40 ± 0.10	360^d	0.72 ± 0.19	9	9.5
HL Tau	04 31 38.4	+18 14 00	< 0.15	5	0.77 ± 0.05	360^d	1.4 ± 0.1	8	15.1
L1489	04 04 43.1	+26 18 58	6.0 ± 0.3	2	2.9 ± 0.2	365	5.3 ± 0.6	8	26.1
L1524	04 26 56.4	+24 43 36	4.5 ± 0.2	2	1.6 ± 0.5	357	2.9 ± 0.9	10	26.9
L1536S	04 33 19.1	+22 46 33	< 1.5	2	0.72 ± 0.15	369	1.3 ± 0.3	8	15.1
L1551 IRS5	04 31 33.9	+18 08 08	5.9	5	2.1 ± 0.2	361	3.8 ± 0.5	8	14.1
L1551NE	04 31 43.5	+18 06 31	3.7 ± 0.8	2	> 2	360^d	> 3.6	10	22.3
TMC1A	04 39 35.0	+25 41 47	6.9 ± 0.4	2	2.4 ± 0.6	360^d	4.3 ± 1.1	10	32.0
Taurus, field stars									
Elias 3	04 23 24.6	+25 00 09	1.95 ± 0.09	1	0.42 ± 0.01	319	0.68 ± 0.07	11	8.4
Elias 6	04 29 07.7	+24 43 50	< 0.3	4	0.27 ± 0.01	335	0.46 ± 0.04	11	6.4
Elias 9	04 32 11.5	+24 33 38	**b**		0.16 ± 0.01	296	0.23 ± 0.03	11	4.4
Elias 13	04 33 25.9	+26 15 34	1.14 ± 0.06	1	0.54 ± 0.01	361	0.97 ± 0.08	11	11.6
Elias 14	04 38 58.3	+26 31 07	< 1.2	4	0.21 ± 0.10	360^d	0.38 ± 0.18	9	5.8
Elias 15	04 39 26.8	+25 52 59	4.6 ± 0.4	3	0.92 ± 0.08	360^d	1.7 ± 0.2	9	15.0
Elias 16	04 39 38.7	+26 11 25	7.4 ± 0.1	1	1.26 ± 0.01	345	2.2 ± 0.2	11	23.5
Elias 17	04 23 24.6	+25 00 09	**b**		< 0.08	360^d	< 0.14	9	4.7
HD28975	04 34 50.0	+24 14 40	**b**		< 0.03	360^d	< 0.05	11	1.5
HD29647	04 41 08.0	+25 59 32	< 0.4	4	0.11 ± 0.01	345	0.19 ± 0.02	11	2.9
HD283701	04 34 54.9	+27 12 12	**b**		< 0.03	360^d	< 0.05	11	1.2
HD283809	04 41 24.9	+25 54 48	**b**		0.08 ± 0.01	312	0.12 ± 0.02	11	5.3
HD283812	04 44 24.8	+25 31 44	**b**		< 0.05	360^d	< 0.09	9	1.8
Tamura 2	04 37 28.3	+26 10 25	**b**		0.26 ± 0.01	329	0.42 ± 0.04	11	6.0
Tamura 8	04 40 58.1	+25 54 16	6.5 ± 0.2	1	1.40 ± 0.08	360^d	2.5 ± 0.3	9	21.5
Tamura 12	04 41 02.8	+25 39 55	**b**		< 0.15	360^d	< 0.27	9	6.3
Tamura 16	04 42 35.6	+25 27 13	**b**		< 0.15	360^d	< 0.27	9	5.7
Tamura 17	04 44 01.5	+25 20 13	**b**		0.06 ± 0.01	312^e	0.09 ± 0.02	11	4.2
Ophiuchus, YSOs									
Elias 21	16 26 21.3	-24 23 02	< 1.2	6	0.8 ± 0.1	360^d	1.4 ± 0.2	12	25.7
Elias 23	16 26 24.1	-24 24 48	< 0.73	6	0.23 ± 0.03	360^d	0.41 ± 0.06	12	17.1(22.6)
Elias 24	16 26 24.2	-24 16 13	< 0.29	6	0.21 ± 0.03	360^d	0.38 ± 0.06	12	12.8
Elias 25	16 26 34.2	-24 23 27	< 1.96	6	0.21 ± 0.03	360^d	0.38 ± 0.06	12	7.3
Elias 27	16 26 44.7	-24 23 07	**b**		0.3 ± 0.1	360^d	0.47 ± 0.16	12	17.4
Elias 29	16 27 09.5	-24 37 21	1.68 ± 0.06	6	1.9 ± 0.1^f	369	3.4 ± 0.3	3	47.8
Elias 30	16 27 10.3	-24 19 12	**b**		0.22 ± 0.03	360^d	0.40 ± 0.06	12	3.0
Elias 32	16 27 28.5	-24 27 17	6.03 ± 0.02	6	1.20 ± 0.15^f	384	2.3 ± 0.3	3	19.0(24.3)
Elias 33	16 27 30.4	-24 27 34	9.5 ± 0.1	6	1.1 ± 0.1^f	376	2.1 ± 0.2	3	22.8(28.1)
WL5	16 27 18.0	-24 28 52	14.0 ± 0.6	6	2.9 ± 0.4	383	5.6 ± 0.9	3	53.3
WL6	16 27 21.4	-24 29 48	8.5 ± 0.2	6	2.0 ± 0.1	361	3.6 ± 0.3	3	51.3(56.6)
WL12	16 26 44.2	-24 34 47	3.36 ± 0.08	6	1.2 ± 0.2	367	2.2 ± 0.4	13	36.7
WL16	16 27 02.1	-24 37 26	0.72 ± 0.16	6	0.9 ± 0.1	338	1.5 ± 0.2	3	25.6(30.9)

Table 1. (continued)

Object	$\alpha(2000)^{a}$	$\delta(2000)^{a}$	$N_s(CO)$ $(10^{17}\,cm^{-2})$	Ref.[g]	τ_{H_2O}	FWHM (cm^{-1})	$N_s(H_2O)$ $(10^{18}\,cm^{-2})$	Ref.[g]	A_V
Ophiuchus, field stars									
Elias 15	16 26 05.8	-24 42 54	< 0.22	6			**c**	12	10.6
Elias 35	16 27 46.7	-24 23 22	< 3.4	6	< 0.05	360[d]	< 0.09	12	12.9
Elias 44	16 33 02.6	-24 22 41	< 2.5	6			**c**	12	7.8
Elias 47	16 38 54.8	-24 11 20	< 0.73	6			**c**	12	9.7

[a] Coordinates from Gezari et al. 1997.
[b] No existing solid CO observations.
[c] No existing estimate for water-ice column density.
[d] Assumed FWHM; see text for details.
[e] Uncertain value: feature contaminated by photospheric OH lines.
[f] Optical depths and uncertainties estimated from spectra in reference 3.
[g] *References:* 1. Digitized from Chiar et al. 1995; 2. Teixeira et al. 1998; 3. Kerr 1994; 4. Whittet et al. 1989; 5. Tegler et al. 1995; 6. Kerr et al. 1993; 7. Whittet et al. 1983; 8. Sato et al. 1990; 9. Whittet et al. 1988; 10. Emerson et al., in prep.; 11. Smith et al.1993; 12. Tanaka et al. 1990; 13. Tanaka et al. 1994

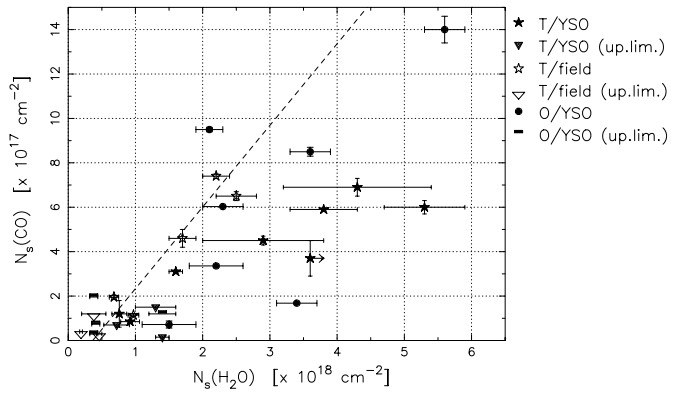

Fig. 1. Solid-CO column density against the solid H_2O column density for all the lines-of-sight listed in Table 1. In the caption with the symbols, Taurus is represented by a T, and Ophiuchus by an O (this nomenclature will be adopted in all figures in the paper). The dashed line represents the linear least-squares fit to the *field stars in Taurus* (excluding the upper limits). See text for details.

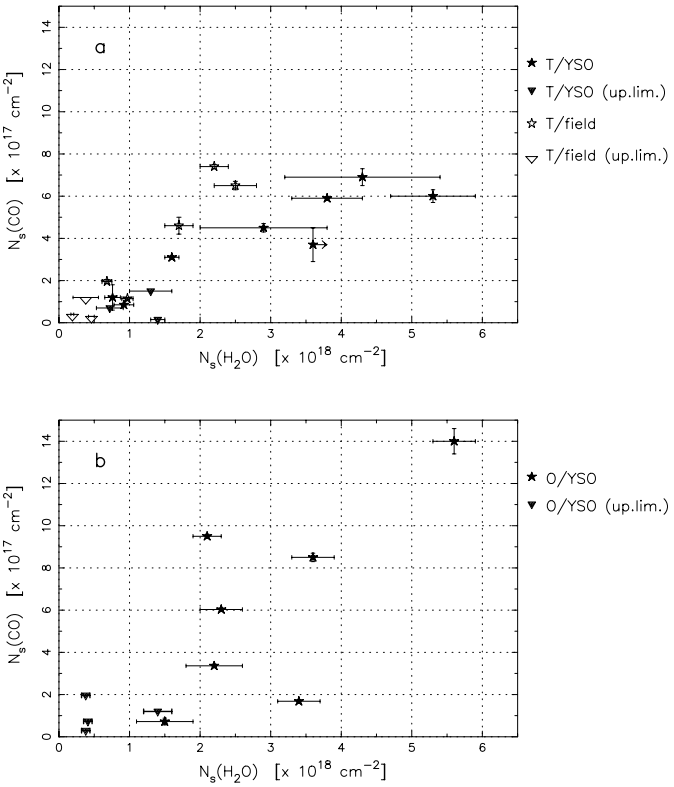

Fig. 2a and b. Solid-CO column density against the solid-H_2O column density for the objects in **a** Taurus, **b** Ophiuchus.

layer of the cloud where only the less volatile, polar mantles can survive the harsh radiation field incident on the cloud (Chiar et al. 1995). From Fig. 1 it is clear that, with the exception of object Elias 33 in Ophiuchus, all objects in Taurus and Ophiuchus where both ices have been detected fall along or below this line. However, this fit is statistically poor, with a reduced-χ^2 of 2.4.

The distinct trends followed by field stars and embedded objects can most easily be seen in Fig. 2a, where only Taurus is plotted. The most striking feature of this plot is the fact that 5 of the 8 embedded YSOs in Taurus show a larger amount of water-ice along their lines-of-sight than any of the lines-of-sight towards field stars, even though the amount of solid-CO is comparable. It seems that the $N_s(CO)/N_s(H_2O)$ ratio is smaller towards embedded objects. A linear least-squares fit (excluding upper limits and the lower limit to L1551NE) gives:

$$N_s(CO) = (0.16 \pm 0.02)\, N_s(H_2O) + (-0.5 \pm 0.4) \times 10^{17}\,cm^{-2}. \quad (3)$$

The average $N_s(CO)/N_s(H_2O)$ ratio in the regions of the cores where both ices can coexist in the lines-of-sight towards YSOs (0.16 ± 0.02) is $\sim 45\%$ lower than that towards field stars. The x-axis intercept is $N_s(H_2O) = (2.8 \pm 1.9) \times 10^{17}\,cm^{-2}$ which, within the errorbars, is coincident with the intercept found for

relation (2) for the field stars. The larger solid-H_2O column densities may be explained if the embedded YSOs are observed through a larger column of material than the field stars. Then, the smaller $N_s(CO)/N_s(H_2O)$ ratio may be due to the embedded young star heating up its surroundings causing the evaporation of the volatile CO mantles while the less volatile H_2O mantles can survive to higher temperatures trapping small amounts of CO in them (Tielens et al. 1991), thereby causing a decrease in that ratio along the line-of-sight.

In the case of Ophiuchus, since there are no field stars with solid-CO, it is not possible to compare trends. The large scatter for the embedded objects is evident in Fig. 2b, even though solid-CO column density increases with solid-H_2O column density. Despite the scatter, a linear regression has also been constructed for Ophiuchus, excluding the upper limits:

$$\begin{aligned} N_s(CO) \;=\; & (0.54 \pm 0.13)\, N_s(H_2O) \\ & +(-7.3 \pm 2.8) \times 10^{17}\,\mathrm{cm}^{-2}. \end{aligned} \quad (4)$$

The average $N_s(CO)/N_s(H_2O)$ ratio in the regions of the cloud where both ices can coexist, 0.54 ± 0.13, is now $\sim$46% larger than that towards field stars in Taurus. The x-axis intercept is $N_s(H_2O) = (14 \pm 2) \times 10^{17}\,\mathrm{cm}^{-2}$, significantly higher than for the objects in or behind Taurus. However, the fit to the data in Ophiuchus is statistically poor, with a reduced-χ^2 of 2.4.

3. The extinction through the clouds

A measurement of the extinction provides an estimate of the amount of dust present along a given line-of-sight. Comparison of the column densities of the ices with the visual extinction, A_v, can provide further clues to the explanation of the differences observed in the previous section.

The A_vs for the objects in Table 1 are derived in a companion paper (Teixeira & Emerson 1999). For most objects, A_v was determined from the (H-K) colour excess, E(H-K). For those objects where H-K colours were not available, A_v was determined from the (J-K) colour excess, E(J-K).

The adopted extinctions, A_v, are presented in Table 1, but have a large degree of uncertainty in absolute terms (perhaps a factor of 2, with a typical uncertainty in A_v of 30%; Teixeira & Emerson 1999). However, by using the same method for the determination of A_v for all the objects, large systematic differences are minimized and their relative positions should be preserved so meaningful comparisons can be made.

3.1. Ices column densities versus extinction

Figs. 3 and 4 are plots of the solid-H_2O and CO column densities, respectively, against the visual extinction, A_v, towards the sources in Table 1. For each of the ices, presenting all the sources in the same plot makes the plots a little complex, but allows easier comparison of different clouds and lines-of-sight. A first analysis of the results will be done taking the joint plots (Figs. 3 and 4), followed by a more detailed analysis of the separate plots for Taurus and Ophiuchus.

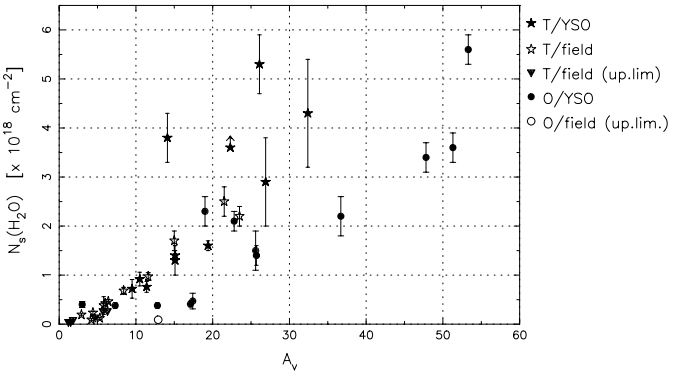

Fig. 3. Solid-H_2O column density against the visual extinction for the sample (Table 1).

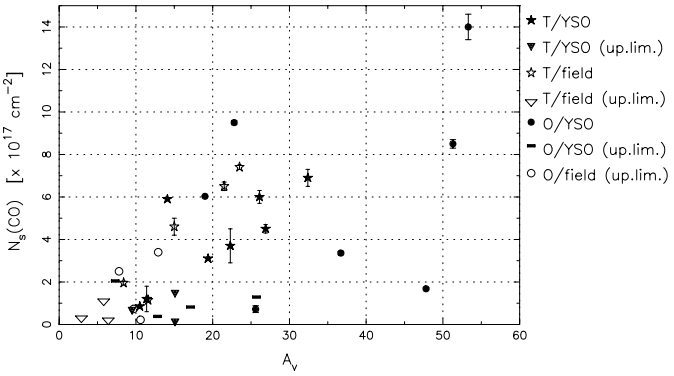

Fig. 4. Solid-CO column density against the visual extinction for the sample (Table 1).

Figs. 3 and 4 highlight the different trends observed towards Taurus and Ophiuchus, making the differences even more conspicuous than in Fig. 1. For $A_v < 14$ mag, the sources in Taurus follow a well defined line in Fig. 3. If that line is extrapolated to higher extinctions, it becomes apparent that, *while the sources in and behind Taurus fall along or above that line, the sources in and behind Ophiuchus fall along or below the line*. The sources in Ophiuchus at extinctions larger than 14 mag which appear to follow such a line are Elias 32, Elias 33 and WL5. Fig. 4 is reminiscent of the joint column densities plot (Fig. 1) in that, while the sources towards Taurus seem to follow some trend(s), the sources towards Ophiuchus appear scattered. This should not be surprising, since three observational parameters are being studied ($N_s(H_2O)$, $N_s(CO)$, and A_v) and two plots are enough to define the relations between the three. Nevertheless, it is useful to analyse the behaviour of each of the ices with the visual extinction for each of the clouds separately.

$N_s(H_2O)$ *versus* A_v for Taurus and Ophiuchus can be seen in Fig. 5. The most striking feature is the high degree of correlation for the sources in Taurus with extinction lower than $\sim$14 magnitudes, but which breaks off for higher extinctions. The tight correlation for the lower extinctions had already been noticed (e.g. Chiar et al. 1995),*but the breaking off of the relation only becomes evident when the deeply embedded sources (Teixeira et al. 1998), not included in previous studies, are con-*

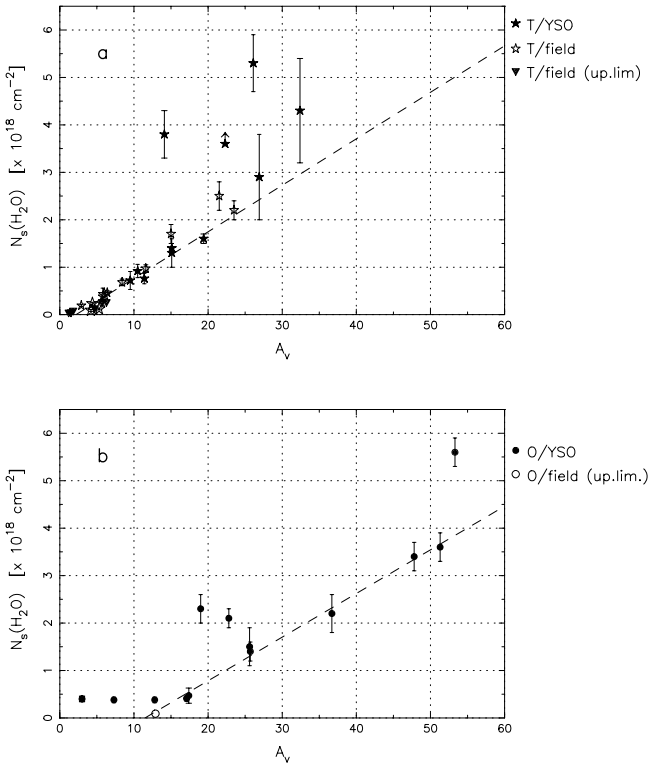

Fig. 5a and b. Solid-H_2O column density against the visual extinction for the objects in **a** Taurus, **b** Ophiuchus. The dashed lines correspond to: **a** linear least squares fit to all the objects with $A_v < 14$ mag, excluding upper limits (Eq. 5), **b** linear least squares fit to the objects with $A_v \geq 15$ mag, excluding the three significantly above the line (Elias 32, Elias 33 and WL5; Eq. (6)).

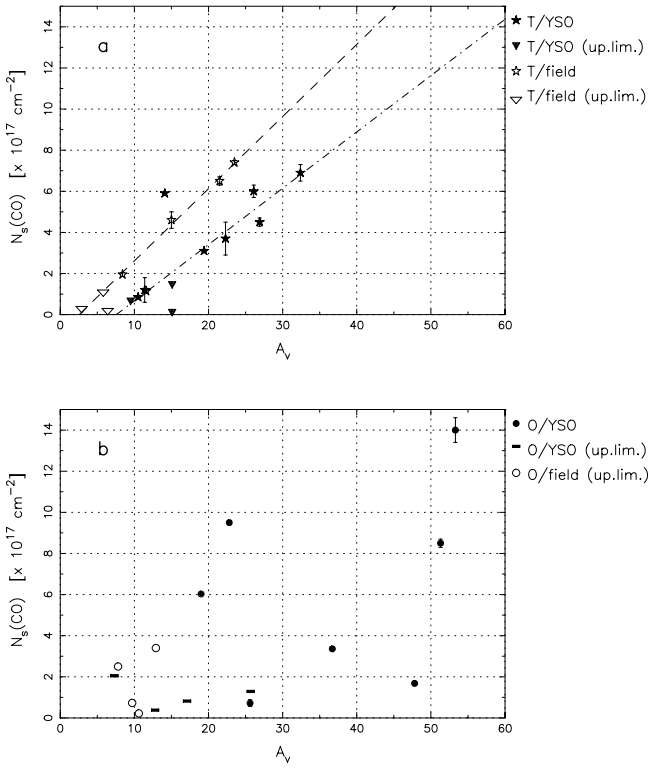

Fig. 6a and b. Solid-CO column density against visual extinction for the objects in **a** Taurus, **b** Ophiuchus. In plot **a**, the dashed line corresponds to a linear least squares fit to the field stars, excluding Elias 13 ($A_v = 11.6$, $N_s(CO) = 1.14 \times 10^{17}\,cm^{-2}$) and the upper limits (Eq. (7)); the dot-dashed line corresponds to a linear least squares fit to the YSOs, excluding L1551 IRS5 ($A_v = 14.1$, $N_s(CO) = 5.9 \times 10^{17}\,cm^{-2}$) and the upper limits (Eq. (8)).

sidered. A linear least-squares fit to the sources in and behind Taurus for which $A_v < 14$ mag (excluding upper limits and without considering uncertainties in the coordinates; Bevington 1969) results in:

$$N_s(H_2O) = [(1.0 \pm 0.1)\, A_V + (-2.1 \pm 0.8)] \times 10^{17}\ cm^{-2} \quad (5)$$

represented by the dashed line in Fig. 5a. Even though *the lines-of-sight to sources embedded in the cloud show a much larger amount of water-ice than expected from relation (5)*, the tendency to larger column densities of solid-H_2O than expected may also be present in the lines-of-sight towards field stars, as evidenced by the displacement of Elias 15 ($A_v = 15.0$, $N_s(H_2O) = 1.7 \times 10^{18}\,cm^{-2}$) and Tamura 8 ($A_v = 21.5$, $N_s(H_2O) = 2.5 \times 10^{18}\,cm^{-2}$) relative to that line. There is a positive intercept on the x-axis[2] of $A^{th}_{V,H_2O} = 2.7 \pm 0.6$. Within the uncertainties, this value is consistent with the value found by Chiar et al. (1995). However, their slope differs somewhat from the value in Eq. (5) mostly due to the fact that Chiar et al. included the 3 field stars (common to both works) with extinctions *larger* than 14 mag (Elias 15, Elias 16, and Tamura 8).

[2] Following the same procedure as in Sect. 2.2, the x-axis intercepts mentioned in this section were obtained by constructing linear least-squares fits to the data taking the column densities as abscissae and A_V as the ordinate.

In the case of Ophiuchus (Fig. 5b), the situation is even less clear. It is tempting to identify a plateau for $A_v \lesssim 15$ mag, as well as a linear relation for larger extinctions. However, three Ophiuchus objects – Elias 32, Elias 33 and WL5 – appear to follow the regression line for objects in Taurus. Excluding those objects, a linear least-squares fit to the objects in Ophiuchus with $A_v \geq 15$ mag results in:

$$N_s(H_2O) = [(0.92 \pm 0.04)\, A_V + (-11 \pm 1)] \times 10^{17}\ cm^{-2} \quad (6)$$

the dashed line in Fig. 5b. The corresponding intercept on the x-axis is $A^{th}_{V,H_2O} = 12 \pm 1$. Within the uncertainties, the slopes of the two regression lines to the objects in Taurus and Ophiuchus ((5) and (6)) are coincident. The interpretation will be addressed in Sect. 4.

The solid-CO column density has a different behaviour with the visual extinction than the solid-H_2O, as seen in the separate plots for Taurus and Ophiuchus in Fig. 6. In Taurus there is a separation between background field stars and embedded YSOs, with the latter showing smaller column densities of CO-ice for the same A_v than the field stars do. Both groups of objects seem to show linear trends of the column density with the extinction, in almost parallel lines. There are exceptions to these trends on both sides, with L1551 IRS5 ($A_v = 14.1$, $N_s(CO) = 5.9 \times 10^{17}\,cm^{-2}$) falling above the field stars, and

with Elias 13 ($A_v = 11.6$, $N_s(CO) = 1.14 \times 10^{17}\,cm^{-2}$) falling among the embedded sources, not to mention some worrying upper limits among the YSOs (HL Tau and L1536S). These problems are addressed in Appendix A.

If a linear least-squares fit is constructed for the field stars towards Taurus, excluding Elias 13 and the upper limits, the result is:

$$N_s(CO) = [(0.35 \pm 0.02)\,A_V + (-0.9 \pm 0.3)] \times 10^{17}\,cm^{-2} \quad (7)$$

represented in Fig. 6a by the dashed line. The corresponding x-axis intercept is $A_{V,CO}^{th} = 2.6 \pm 0.8$. If Elias 13 is considered, the slope increases slightly but is equal to the slope in relation (7) within the uncertainties, while the intercept increases to $A_{V,CO}^{th} = 6 \pm 2$. However, in both cases Elias 13 appears as an outlier to the regression line. Within the uncertainties, relation (7) is consistent with the result obtained by Chiar et al.(1995); when Elias 13 is included in the fit, the results are almost coincident.

The dot-dashed line in the same figure corresponds to the linear least-squares fit to the embedded YSOs in Taurus, excluding L1551 IRS5 and the upper limits:

$$N_s(CO) = [(0.27 \pm 0.03)\,A_V + (-2.1 \pm 0.7)] \times 10^{17}\,cm^{-2}. \quad (8)$$

In this case the x-axis intercept is $A_{V,CO}^{th} = 8.3 \pm 1.6$. From relations (7) and (8) we conclude that the two regression lines have marginally different slopes, but the x-axis intercepts are different by a factor of ~ 3.

For Ophiuchus, the scatter in Fig. 6b is so large that it is not possible to identify any trend. Note there are only upper limits (though some of them not very stringent) of solid-CO for extinctions lower than ~ 18 magnitudes.

4. Interpretations of the results

Plots and results like those presented in Sects. 2.2 and 3.1 can help to understand the conditions in molecular clouds and the mechanisms controlling mantle formation and survival (e.g. Sato et al. 1990, Tanaka et al. 1990, Williams et al. 1992, Duley & Smith 1995, Chiar et al. 1995). However, such results must be regarded with great caution in view of the large uncertainties associated with the quantities involved, and because it is dangerous to do statistics on small numbers of lines-of-sight (typically between 4 and 12, in the cases of Taurus and Ophiuchus). A detailed discussion of the problems and uncertainties can be found in Appendix A, and we adopt conclusions about the uncertainties in the suggested relations from it.

The following section presents an analysis of Figs. 1 to 6 assuming the linear relations are real, while Sect. 4.2 presents a preferred alternative view.

4.1. The linear relations

Within the uncertainties, the slopes of the regression lines corresponding to the relation between $N_s(H_2O)$ and A_v for Taurus and Ophiuchus (expressions (5) and (6) respectively) are identical, as previously noted by Smith et al. (1993). Thus for both clouds the average number of H_2O molecules per dust grain is the same, which might suggest similar grain and mantle size distributions, and similar mechanisms of mantle growth and survival in the two clouds.

A common point to all the relations between the ices' column densities and the visual extinction (expressions (5), (6), (7) and (8)) is the existence of positive intercepts on the A_v-axis. These intercepts, A_{V,H_2O}^{th} and $A_{V,CO}^{th}$, are threshold extinctions below which the H_2O and CO mantles, respectively, cannot survive (e.g. Whittet et al. 1988, 1989). The existence of such thresholds led Whittet et al. to conclude that a minimum visual extinction is required for the grains to be sufficiently shielded from the interstellar radiation field incident on the clouds and for the ice mantles to be able to survive. In fact, Williams et al. (1992) showed that the threshold for water-ice may be determined by the local IR radiation field near 3 μm in each cloud. Such a mechanism could explain the different values of A_{V,H_2O}^{th} observed towards different dark clouds (e.g. Chiar et al. 1995 for Taurus, Tanaka et al. 1990 for Ophiuchus, Eiroa & Hodapp 1989 for Serpens, Chen & Graham 1993 for Corona Australis) as due to different strengths of the ambient IR radiation field (Williams et al. 1992). As those authors point out, the same type of mechanism could also be responsible for the existence of the threshold extinction for the survival of CO-ice mantles, $A_{V,CO}^{th}$ (e.g. Chiar et al. 1995 for Taurus, Kerr et al. 1993 for Ophiuchus, Chiar et al. 1994 for Serpens).

4.1.1. The H_2O threshold

In the case of $N_s(H_2O)$ *versus* A_v in Taurus, even though the scatter for large values of A_v is large, for $A_v < 14$ mag there appears to be a high degree of correlation making A_{V,H_2O}^{th} for this cloud reasonably well defined, as previously seen. The situation for Ophiuchus, however, is far from clear. Even though the linear regression points to a value of $A_{V,H_2O}^{th} \sim 12$ mag, two of the objects defy this limit down to ~ 3 magnitudes of extinction. To bring them near the correlation line it would be necessary to suppose that their visual extinctions had been underestimated by a factor of 2 because of scattered light at H and K, for example, and also that Elias 30 should have the intrinsic colour of a Class III source rather than a Class I or II. This would be possible, but difficult to reconcile with the fact that Elias 30 is observed to have hot circumstellar dust (Wilking et al. 1989) and that modelling of its SED results in a value of $A_v = 5$ mag (Adams et al. 1987). An alternative explanation was proposed by Tanaka et al. (1990), who first noticed sources in Ophiuchus which violated the existence of a threshold extinction. According to Tanaka et al., a linear relation like that presented in Fig. 5b would only apply to the protostars (the most embedded objects, which may be identified with the Class I sources) and to the field stars, but not to the more evolved "emission-line" stars (which may be identified with classical T Tauri stars, Class II objects, as Elias 30 is classified) and to the early type stars (as Elias 25 is classified). Tanaka et al. also noticed that their "emission-line"

stars (including Elias 23, 24, 27 and 30) have roughly similar amounts of water-ice in their lines-of-sight, which they interpreted as evidence for icy circumstellar disks of almost equal size around those sources. Even if one supposed that the sizes and structures of the disks surrounding classical T Tauri stars were all similar (despite the fact that those 4 objects have luminosities differing up to a factor of ~ 100), it is difficult to understand why the emission-line stars of the sample in Ophiuchus are all seen in the same geometry (when a star+disk system is highly spherically *asymmetric*), and why the emission-line stars in Taurus (as, for example, HL Tau) appear to have much larger disks. It is therefore unclear, from the observations, what the threshold extinction for the survival of the H_2O-ices in Ophiuchus is: whether ~ 12 mag as derived from the linear fit to some of the objects, or ~ 3 mag as in the case of Taurus.

As suggested by de Geus (1992), the original Ophiuchus cloud may have been disrupted by the violent evolution of the massive stars in the Upper-Scorpius association. Due to a shock caused by a supernova explosion in Upper-Scorpius, and to stellar winds being blown by the early-type stars in that association, a large part of the material of the original Ophiuchus cloud may have been swept away and deposited behind the cloud, which happens to be in the direction of the Earth. The star formation in ρ-Ophiuchi, the main, star-forming core of the Ophiuchus complex (e.g. Loren et al. 1990), may then have been triggered by the encounter between the expanding shock and that dense clump. The lower density material in the clump may have been swept away to form what today is seen as the "streamers", and the ρ-Ophiuchi clump may today be part of a "nose" of material which stayed behind the shock, sticking into the shell blown by the massive stars in the Upper-Scorpius association (see Fig. 11 of de Geus 1992). As a consequence of the passage of the shock through the clump and/or of the strong radiation field from the early-type stars in Upper-Scorpius and from the forming stars in ρ-Ophiuchi itself, the ice mantles in that "nose" might not have survived, leaving the grains bare and causing the 12 magnitudes threshold extinction for the water-ice. Then, the objects that violate that threshold could correspond to lines-of-sight which do not cross the region affected by the strong radiation field and/or shock.

4.1.2. The CO threshold

A threshold extinction for the detection of solid-CO poses even more problems than that for solid-H_2O. For Taurus, even though there appear to be linear relations between N_s(CO) and A_v, the scarcity of sources at low extinctions (in particular for the field stars) makes it difficult to ascertain whether the threshold indeed corresponds to the A_v-axis intercept given by each linear regression, or if, instead, there is a sharp cut-off at a value of A_v higher than the intercept (both for the field stars and the YSOs). In any case, the threshold value of extinction appears to be larger for the embedded YSOs than for the field stars. This is actually as expected, though contrary to what was stated by Whittet et al. (1988), as the embedded young stars are surrounded by dense envelopes which are heated by the forming star at its centre. Close to the star, the temperature is too high for any grains to survive but, beyond a certain radius, the temperature drops enough for bare grains to exist and, further out, for ice mantles to survive on the grains. Because both the density and the temperature of the envelope increase inwards, there will be extra visual extinction (relative to the field stars) contributing to the threshold, corresponding to the inner regions of the envelope which are too hot for the ices to survive. Such a view does not seem to apply to the water-ice. As can be seen in Fig. 5a, the embedded YSOs follow the same trend as the field stars for $A_v < 14$ mag. The reason for the difference may be that CO-ice is much more volatile than H_2O-ice (pure CO sublimes at ≈ 15–20 K under astrophysical conditions, and pure-H_2O at ≈ 100–150 K (e.g. Sandford et al. 1988), and therefore more sensitive to the presence of the warm envelope than the water-ice.

4.1.3. Implications

If the value of the threshold extinction for the survival of the ices is given by the A_v-axis intercept for each of the linear fits, then, for the field stars behind Taurus, the values of the threshold extinctions for CO and H_2O are identical. This causes a problem to the scenario of the "layered" structure of the Taurus cloud, as suggested by Kerr (1994), in which there would be an outer layer of the cloud where grains are unmantled (presumably because of the harsh, external radiation field), then a layer where the ice mantles consist mostly of H_2O, and finally the protected, inner regions of the cloud where the grains have both H_2O and CO ice mantles. The layer where no ices exist would be responsible for the A^{th}_{V,H_2O}, and the sum of that with the extinction due to the layer where only H_2O-ices can exist would produce the $A^{th}_{V,CO}$. The existence of the thresholds means that there is an outer "skin" of the cloud where ice mantles are absent from the grains, but the equality of the two thresholds then means that CO-ices are always found where H_2O-ices are present. That is possible if the CO molecules in the mantles in the outer regions of the cloud are trapped in the H_2O mantles, making it possible for CO-ices to survive in conditions where pure CO ice would sublime.

In the case of Ophiuchus the situation is even more difficult to understand, in view of the large scatter and lack of any acceptable relation between the column density of CO-ice and the visual extinction. Kerr et al. (1993) suggested that the scatter could be evidence for the influence of the embedded young stars in their surroundings, causing variations of the CO band strength. Whether that is so or not is hard to assess. The fact that the scatter is not as large in Taurus may be explained by the fact that Ophiuchus forms higher mass stars relative to Taurus, causing a larger disruption of the ambient cloud. Further support for the explanation proposed by Kerr et al. (1993) comes from the fact that all of the sources in Ophiuchus with the largest column densities of CO-ice (N_s(CO)$> 4 \times 10^{17}$ cm^{-2}) are not detected at 1.3 mm (Motte et al. 1998). That means that, in those lines-of-sight, there is no evidence for the presence of warm and cold envelope dust heated by the underlying forming stars. Also, 3

of those 4 YSOs appear to roughly follow the regression lines to the field stars in Taurus both in the case of water-ice and CO-ice.

4.2. The $A_v \sim 15$ mag discontinuity

An alternative interpretation of the plots may be adopted. Rather than assuming that linear relations between $N_s(CO)$, $N_s(H_2O)$, and A_v exist, there might be discontinuities, as already pointed out when comparing the column densities of CO and H_2O ices (Sect. 2.2). In the case of Taurus, the plot of $N_s(H_2O)$ versus A_v (Fig. 5a) has a discontinuity at $A_v \sim 15$ mag (where $N_s(H_2O) \sim 1.5 \times 10^{18}$ cm^{-2}, which is the same as the H_2O-ice column density where the plot of $N_s(CO)$ against $N_s(H_2O)$ appeared to show a discontinuity). What might be happening at 15 magnitudes of visual extinction to cause the discontinuity? Perhaps the "water-ice enhancement" occurs only for the embedded YSOs, as a consequence of chemical changes taking place due to the influence of the forming star. Bergin et al. (1995) showed that, when they simulated a star "turn on" in their gas-grain chemical model, the abundance of gas-phase H_2O increased with time and that, in some cases, the amount of H_2O *in the mantles* could also increase with time. That increase of the abundance of solid-H_2O is highly dependent on the assumed temperature of the dust (the increase occurs for $T_{dust} = 25$ K, but for $T_{dust} = 30$ K it is no longer observed), and only becomes perceptible at times later than $\sim 10^6$ yr, which is also a problem since Class I objects have estimated ages of $\sim 10^5$ yr (Kenyon et al. 1993, André & Montmerle 1994, Kenyon & Hartmann 1995). If, however, the H_2O formed in the gas-phase were condensed on the grains, such an enhancement of water-ice on the grains could take place.

Another possibility is that the discontinuity occurs both for YSOs and for field stars, and reflects a transition between two regimes of H_2O desorption from (or condensation onto) the grains. The surface binding energy of H_2O on unannealed pure H_2O has been measured by Sandford & Allamandola (1988) to be ~ 0.415 eV, corresponding to radiation with wavelength $\sim 3\,\mu$m. Taking the average R_v-dependent extinction law parameterized by Cardelli et al. (1989) with $R_v = 3.6$, then, for an optical depth of unity at $3\,\mu$m, the corresponding visual extinction is $A_v \approx 14.9$ mag. This coincides with the value of A_v at which the linear relation between $N_s(H_2O)$ and A_v in Taurus breaks down. It may be that, below ~ 15 magnitudes of extinction, the growth of the H_2O mantles is restricted by the incident radiation around $3\,\mu$m; above ~ 15 magnitudes, the shielding from the penetrating radiation may be enough to allow the ice mantles to grow larger. Then the scatter observed in Figs. 2, 5 and 6 may reflect this discontinuity, rather then just uncertainties and systematic errors in the observations and calculations. This interpretation also provides support for the role of the local radiation field around $3\,\mu$m in the survival of the ice mantles in the cloud (Williams et al. 1992) However, Cardelli et al.'s extinction law does not have the H_2O-ice feature built into it. Since at $\sim 3.1\,\mu$m there will be the extra contribution of that feature to the extinction, the value of A_v for optical depth unity at $3\,\mu$m previously derived using Cardelli et al.'s extinction law will overestimate A_v.

4.3. On the lines-of-sight to field stars

Relation (5) between $N_s(H_2O)$ and A_v in Taurus, for $A_v \leq 12$ mag, should define an upper limit to the water-ice column density measured along a given line-of-sight, rather than a strict relation between the two parameters applying especially to the field stars. In fact, the visual extinction measured from an observer on Earth along a given line-of-sight defines an upper limit to the minimum extinction in all directions for any grain in the cloud along that line-of-sight. That is so because a molecular cloud is a 3-dimensional system and so, even for a grain in the middle of that path, the visual extinction to the nearest embedded source of radiation may be smaller than the visual extinction to the edges of the cloud. Grains in a line-of-sight to a background field star may in this way also feel the effects of a nearby forming star. It should therefore not be taken for granted that lines-of-sight towards background field stars necessarily sample quiescent regions of a cloud, undisturbed by the process of star formation, as is often thought.

5. Conclusion

We have compiled and compared the results of observations of H_2O and CO ices towards the Taurus and Ophiuchus dark clouds. The aim was detecting and interpreting similarities and/or differences between the results for those nearby star-forming complexes.

To a great extent we confirm previous results and interpretations, namely that Taurus and Ophiuchus sample regions of different physical conditions, and that the column densities of the ices and the visual extinction are inter-correlated. However, it is shown that, contrary to what was previously stated, it is not clear that the two clouds have different or well defined threshold extinctions for the survival of ice mantles, nor that, for each of the clouds, the thresholds for the survival of CO and H_2O mantles are different. Moreover, the inclusion of the deeply embedded YSOs observed in this work resulted in a previously unnoticed large scatter, larger than can be accounted for by the observational uncertainties. That is most clear in the case of solid H_2O in Taurus.

For $A_v < 14$ mag there is a tight correlation between the column density of water-ice and the A_v. At $A_v \sim 15$ magnitudes there is a discontinuity above which the scatter in the plot increases and that correlation seen for $A_v < 14$ mag disappears. This discontinuity is also apparent in the relation between the column densities of the two ices, H_2O and CO. One interpretation is that the discontinuity occurs at the value of A_v for which the optical depth at $3\,\mu$m (the wavelength of the H_2O-ice absorption feature) is unity, reflecting a transition between two regimes of H_2O desorption from (or condensation onto) the grains. This may provide support to the hypothesis of the role of the radiation field around $3\,\mu$m local to the cloud, on the

regulation of the formation and survival of the ice mantles in the clouds (Williams et al. 1992).

Acknowledgements. Tom Kerr is gratefully acknowledged for providing his CO- and H_2O-ice data in Ophiuchus. TCT acknowledges support from JNICT, Portugal, in the form of grants CIENCIA/BD/2095/92-RM and PRAXIS XXI/BD/5622/95. This work has made use of the *SIMBAD* database, operated at *CDS*, Strasbourg, France.

Appendix A: deviations from the mean relationships

If the linear relations between $N_s(CO)$ and $N_s(H_2O)$ (expressions (2), (3), and (4)), $N_s(H_2O)$ and A_v (expressions (5) and (6)), and $N_s(CO)$ and A_v (expressions (7) and (8)) are real, it is necessary to explain why some of the objects seem not to follow such relations.

A.1. H_2O *v.s* A_v

For Taurus (Fig. 5a), the most important fact to notice is the scatter for $A_v \gtrsim 14$ mag.

This could be explained if the solid-H_2O column densities for (some of) the objects had been incorrectly estimated. However, it is difficult to explain why the column densities of the objects that do not follow the regression line (5) have all been consistently overestimated, and even taking the errorbars in Table 1 (which already account for the uncertainties in the peak optical depth and width of the H_2O features) 5 of the points still lie above that line.

Another explanation could be that the visual extinctions to those sources were underestimated. This might be true for the embedded YSOs, as a large part of the radiation at H and K might be light scattered into the beam, but that problem should not affect the background field stars. In any case, it is difficult to understand why 6 of the 11 embedded sources appear not to be affected at all by scattering of radiation into the beam.

In the case of Ophiuchus (Fig. 5b), the same problems could occur causing some of the objects to fall well above the regression line. Again, taking into account the errorbars, the objects still fall above the line. Even if five of the objects in Ophiuchus are reclassified as highly obscured Class III objects[3], the scatter for $A_v > 20$ mag is still large and, although there is a tendency for larger column densities with increasing A_v, it is difficult to find an acceptable linear relation between the two quantities with the available measurements.

A.2. CO v.s A_v

The relation between $N_s(CO)$ and A_v brings further problems. Starting with the field stars in Taurus, the most noticeable fact is the displacement of Elias 13 ($A_v = 11.6$, $N_s(CO) = 1.14 \times 10^{17}\,cm^{-2}$, $N_s(H_2O) = 0.97 \times 10^{18}\,cm^{-2}$) relative to the regression line for the field stars (expression (7), Fig. 6a). While Elias 3 ($A_v = 8.4$, $N_s(CO) = 1.95 \times 10^{17}\,cm^{-2}$, $N_s(H_2O) = 0.68 \times 10^{18}\,cm^{-2}$) follows the regression line for solid-CO and Elias 13 does not, they *both* follow the regression line for solid-H_2O (Fig. 5a, expression (5)). Decreasing A_v for Elias 13 (or increasing it for Elias 3) would mean they would then not follow the regression line for solid-H_2O which they now appear to follow very closely. Another problem is Elias 6 ($A_v = 6.4$, $N_s(CO) < 0.3 \times 10^{17}\,cm^{-2}$, $N_s(H_2O) = 0.46 \times 10^{18}\,cm^{-2}$), whose upper limit on $N_s(CO)$ falls well below the regression line (7), but follows the regression line for water-ice (expression (5), Fig. 5a). For the embedded sources, the problems are also clear: while L1551 IRS5 ($A_v = 14.1$, $N_s(CO) = 5.9 \times 10^{17}\,cm^{-2}$, $N_s(H_2O) = 3.8 \times 10^{18}\,cm^{-2}$) is far above the regression line for the YSOs (relation (8)), the upper limits on $N_s(CO)$ for L1536S ($A_v = 15.1$, $N_s(CO) < 1.5 \times 10^{17}\,cm^{-2}$, $N_s(H_2O) = 1.3 \times 10^{18}\,cm^{-2}$) and HL Tau ($A_v = 15.1$, $N_s(CO) < 0.15 \times 10^{17}\,cm^{-2}$, $N_s(H_2O) = 1.4 \times 10^{18}\,cm^{-2}$) place them significantly below that line (Fig. 6a). For L1551 IRS5, it could be argued that its visual extinction has been underestimated for the reasons explained above. It could also be that the solid-CO column densities were incorrectly estimated for L1551 IRS5 and for Elias 13, but it is difficult to justify factors of 2 or larger given the quality of the observations. The problem for the other two objects, L1536S and HL Tau, seems to be more severe, since they too appear to follow the regression line for water-ice rather closely: lowering their A_v in order to be consistent with the regression line for solid-CO would bring them far above the regression line for solid-H_2O. The location of HL Tau in Fig. 5a might be explained if the absorption arises in a circumstellar disk rather than in an envelope (Cohen 1983, Whittet et al. 1989, Mundy et al. 1996), where the temperature might be low enough for the H_2O ices to survive but too high for the CO ices to survive. Then, L1536S could perhaps be a similar case.

A.3. CO v.s H_2O

Correlations between $N_s(CO)$ and $N_s(H_2O)$ are not very tight in view of the scatter of the points in Fig. 2. Even when the (large) uncertainties in the column densities are considered, the scatter is still too large. In Taurus, the field stars Elias 3 and Elias 13 deviate significantly from the regression line (2). Their column densities may have been incorrectly estimated but, as already explained, that would cause problems with the relation between $N_s(H_2O)$ and A_v, and incorrect estimates of the column densities by a factor of 2 or larger are difficult to reconcile with the quality of the observations. In the case of the embedded YSOs in Taurus, Elias 18 and HL Tau deviate significantly from the regression line (3). The case of HL Tau has been discussed above. For Elias 18 ($A_v = 19.4$, $N_s(CO) = 3.1 \times 10^{17}\,cm^{-2}$, $N_s(H_2O) = 1.6 \times 10^{18}\,cm^{-2}$), moving it to the regression line (3) would quite obviously move it away from the regression lines (5) and (8). It can, of course, be argued that the column density estimates for that object are correct and that the problem is that the water-ice column densities of the objects with the

[3] Elias 23, 32 and 33, WL6 and WL16; the values of the extinction corresponding to such a reclassification are given in parenthesis in Table 1) (Teixeira 1998)

largest values of $N_s(H_2O)$ are overestimated, but the problems associated with that have already been mentioned above.

References

Adams F.C., Lada C.J., Shu F.H., 1987, ApJ 312, 788
André P.A., Montmerle T., 1994, ApJ 420, 837
Bergin E.A., Langer W.D., Goldsmith P.F., 1995, ApJ 441, 222
Bevington P.R., 1969, Data Reduction and Error Analysis for the Physical Sciences. McGraw-Hill
Boogert A.C.A., Schutte W.A., Helmich F.P., Tielens A.G.G.M., Wooden D.H., 1997, A&A 317, 929
Cardelli J.A., Clayton G.C., Mathis J.S., 1989, ApJ 345, 245
Chen W.P., Graham J.A., 1993, ApJ 409, 319
Chiar J.E., Adamson A.J., Kerr T.H., Whittet D.C.B., 1994, ApJ 426, 240
Chiar J.E., Adamson A.J., Kerr T.H., Whittet D.C.B., 1995, ApJ 455, 243
Chiar J.E., Gerakines P.A., Whittet D.C.B., et al., 1998, ApJ 498, 716
Cohen M., 1983, ApJ 270, L69
Draine B.T., 1995, Ap&SS 233, 111
Duley W.W., Smith R.G., 1995, ApJ 450, 179
Eiroa C., Hodapp K.W., 1989, A&A 210, 345
Gerakines P.A., Schutte W.A., Greenberg J.M., van Dishoeck E.F., 1995, A&A 296, 810
de Geus E.J., 1992, A&A 262, 258
Gezari D.Y., Pitts P.S., Schmitz M., 1997, Catalog of Infrared Observations. Ed. 4, http://cdsweb.u-strasbg.fr/viz-bin/Cat?II/216
de Graauw Th., Whittet D.C.B., Gerakines P.A., et al., 1996, A&A 315, L345
Gürtler J., Henning Th., Kömpe C., Pfau W., Krätschmer W., Lemke D., 1996, A&A 315, L189
d'Hendecourt L.B., Allamandola L.J., 1986, A&AS 64, 453
d'Hendecourt L.B., de Muizon M.J., 1989, A&A 223, L5
Kenyon S.J., Hartmann L.W., 1995, ApJS 101, 117
Kenyon S.J., Whitney B.A., Gomez M., Hartmann L.W., 1993, ApJ 414, 773
Kerr T.H., 1994, Ph.D. Thesis, University of Central Lancashire
Kerr T.H., Adamson A.J., Whittet D.C.B., 1993, MNRAS 262, 1047
Loren R.B., Wootten A., Wilking B.A., 1990, ApJ 365, 269
Mathis J.S., 1990, ARA&A 28, 37
Mathis J.S., 1993, Rep. Prog. Phys. 59, 605
Mathis J.S., 1998, ApJ 497, 824
Motte F., André P., Neri R., 1998, A&A 336, 150
Mundy L.G., Looney L.W., Erickson W., et al., 1996, ApJ 464, L169
Palumbo M.E., Geballe T.R., Tielens A.G.G.M., 1997, ApJ 479, 839
Press W.H., Teukolsky S.A., Vetterling W.T., Flannery B.P., 1992, Numerical Recipes. The Art of Scientific Computing. 2nd ed., Cambridge University Press
Sandford S.A., Allamandola L.J., 1988, Icarus 76, 201
Sandford S.A., Allamandola L.J., Tielens A.G.G.M., Valero L.J., 1988, ApJ 329, 498
Sato S., Nagata T., Tanaka M., Yamamoto T., 1990, ApJ 359, 192
Schutte W.A., 1996, In: Greenberg J.M. (ed.) The Cosmic Dust Connection. Kluwer Academic Publishers, p. 1
Smith R.G., Sellgren K., Brooke T.Y., 1993, ApJ 263, 749
Strazzulla G., Nisini B., Leto G., Palumbo M.E., Saraceno P., 1998, A&A 334, 1056
Tanaka M., Sato S., Nagata T., 1990, ApJ 352, 724
Tanaka M., Nagata T., Sato S., Yamamoto T., 1994, ApJ 430, 779
Tegler S.C., Weintraub D.A, Rettig T.W., et al., 1995, ApJ 439, 279
Teixeira T.C.V.S., 1998, CO-ices in embedded Young Stellar Objects. Ph.D. Thesis, Univ. of London. Available on-line at http://www.obs.aau.dk/∼tct/
Teixeira T.C., Emerson J.P., 1999, A&A 351, 303
Teixeira T.C., Emerson J.P., Palumbo M.E., 1998, A&A 330, 711
Tielens A.G.G.M., Allamandola L.J., 1987a, In: Hollenbach D.J., Thronson H.A. (eds.) Interstellar Processes. Kluwer, p. 397
Tielens A.G.G.M., Allamandola L.J., 1987b, In: Morfill G.E., Scholer M. (eds.) Physical Processes in Interstellar Clouds. NATO-ASI C210, Reidel, p. 333
Tielens A.G.G.M., Tokunaga A.T., Geballe T.R., Baas F., 1991, ApJ 381, 181
Whittet D.C.B., Bode M.F., Longmore A.J., Baines D.W.T., Evans A., 1983, Nat 303, 218
Whittet D.C.B., Bode M.F., Longmore A.J., Adamson A.J., McFadzean A.D., 1988, MNRAS 233, 321
Whittet D.C.B., Adamson A.J., Duley W.W., Geballe T.R., McFadzean A.D., 1989, MNRAS 241, 707
Whittet D.C.B., Gerakines P.A., Tielens A.G.G.M., et al., 1998, ApJ 498, L159
Wilking B.A., Lada C.J., Young E.T., 1989, ApJ 340, 823
Williams D.A., 1993, In: Millar T.J., Williams D.A. (eds.) Dust and chemistry in Astronomy. IOP Publ. Ltd., p. 143
Williams D.A., Hartquist T.W., Whittet D.C.B., 1992, MNRAS 258, 599